Transactions on Modelling and Simulation vol 20, © 1998 WIT Press, www.witpress.com, ISSN 1743-355X

3-D impedance tomography of high contrast objects

H.N. Oğuz[a] & David Han[b]
[a]*Department of Mechanical Engineering, The Johns Hopkins University, Baltimore, Maryland 21218, USA*
[b]*Applied Physics Laboratory, The John Hopkins University Laurel, Maryland 20723, USA*

Abstract

An algorithm for imaging high contrast objects is developed by means of a 3-D boundary integral method. In the model problem, a conductive cylinder with embedded voids is considered. Simulated measurement points are placed on a band around the mid section of the cylinder, and a given distribution of an electric potential is applied. Starting with initial void shapes and locations, a forward problem is solved with a boundary integral method. The difference between the computed and measured fluxes at the electrodes are minimized by a Levenberg-Marquardt algorithm. The shapes of the voids are parameterized to reduce the degrees of freedom of the system, and to stabilize the inversion process. Numerical simulations show that spheroidal voids can be accurately imaged with a single voltage pattern.

Introduction

The general problem of Electrical Impedance Tomography (EIT) consists in the reconstruction of an unknown impedance distribution in a spatial region on the sole basis of measurements on the boundary. The technique, originally developed for biomedical and geological applications, uses an array of electrodes placed on the boundary of the domain of interest. Predetermined voltages (or currents) are applied

to these electrodes, and the resulting currents (or voltages) are measured. Upon collecting the measurements, the central problem of EIT is how to use the information to reconstruct the impedance distribution in the region. The problem that arises in this way falls in the category of so-called inverse problems as the solution sought is not the calculation of currents (or voltages), given voltages, (or currents) and the parameters of the domain – as in the direct problem – but the specification of the domain parameters itself. It is well known that problems of this type are often ill posed because the solution does not depend continuously on the data: a change in the data, such as small amounts of measurement noise, are sufficient to greatly affect the resolution. It is therefore essential to stabilize the solution against the instability resultant from noisy data.

In general, the approaches developed to date to determine the unknown impedance distribution fall into two classes. One is the so-called back-projection method, which is basically an adaptation of the technique developed for medical CAT-scans. This method has been developed under the assumption that the impedance contrast in the region is small and is therefore not suitable when the conductivity differences in the medium are very large as in the case considered here. The other so called "model based" approach consists in the generation of a sequence of solutions of the direct, or forward, problem, in which the currents (or voltages) predicted on the basis of an assumed impedance distribution are compared with those measured. The forward part consists of the numerical solution of a boundary value problem with the assumed impedance distribution. At each step the assumed impedance distribution is refined in such a way as to decrease the mismatch between direct solution and measurement. There are variations in the numerical technique available for the forward problem. Dines and Lytle [2] used a resistor network to discretize the domain for mapping resistivity within geological core samples. Cheney et al. [1] employed a finite difference technique for the domain discretization. Wexler and Neuman [11] and Murai and Kagawa [9] used a finite element technique for their forward problem solution. Wexler and Neuman's work included both two and three-dimensional cases, and also an experiment. But the computer implementation required an excessive number of iterations to converge to the correct image (1700 in one example), and it exhibited solution instabilities even with ideal measurement data. Murai and Kagawa

limited their study to two-dimensional cases and included measurement error considerations. Singular Value Decomposition (SVD) was used to handle the solution sensitivity to measurement errors. Reasonable results were achieved with their scheme. Murai and Kagawa [8] later extended the work using the boundary element discretization technique. More recently, Jones et al. [7] applied the finite element method in the forward problem to image two-dimensional binary mixture flows. Their work included experiments and comparison to a back-projection method developed by Guardo et al. [4].

In this study, a special class of EIT problems is addressed, in which the region of interest is a three-dimensional cylinder, and the unknown electrical conductivity can only take the values 1 and 0. In other words, the region of interest is composed of a conductive cylindrical medium containing voids of zero conductivity. Measurements are at very low frequency so that the impedance is purely real and reduces to the resistivity. Thus it can be stated that the objective here is not to compute the domain impedance distribution as in a typical EIT problem, but to image the boundary of the voids in the domain. To take advantage of the special nature of the case, a model based technique with the boundary integral method for the forward problem, and the Levenberg-Marquardt type algorithm for the inverse problem is employed.

One of the persistent problem in the model based approach is that the system to be solved in the iteration procedure often becomes singular or nearly so. The degree of ill conditioning of the matrix depends, among others, on the ratio of the number of measurements versus the number of unknowns. If the ratio between these two quantities is low - i.e., a relatively small number of measurements in relation to the number of unknowns describing the image - the matrix becomes highly ill-conditioned. Thus a sensible solution is to describe an image using as a small number of parameters as possible. In this work this is accomplished by the shape parameterization technique. Past workers used a representation of the object outline in terms of a certain number of points from which the surface was reconstructed by interpolation. We have found that an alternative approach may be much more robust and gives rise to much better conditioned matrices. We call this approach "shape decomposition," as the object outline is approximated as a linear combination of fundamental "shapes."

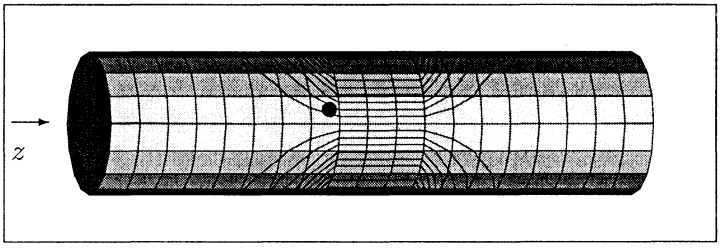


Figure 1: The boundary integral grid of the conductive cylinder. Contours of the electric potential are shown on the cylinder surface.

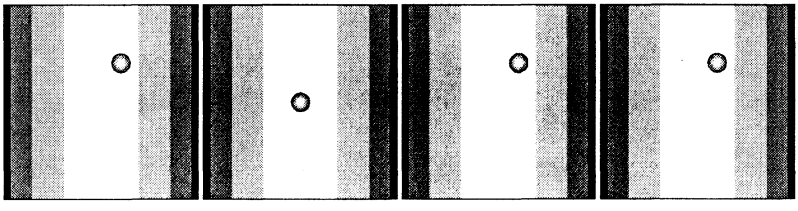


Figure 2: Images of the voids on the $x - z$ plane. Frame 1: original void, 2: initial guess, 3: intermediate, and 4: reconstructed void. The shape parameters are $x = 1, y = 1, z = 1$, $a_{00} = 0.5$ (original and reconstructed).

The advantage of using the boundary element technique in the forward step of a problem such as this is obvious. The unknowns in the forward problem are quantities residing only on the boundary of the domain. Since the surface of the voids is the domain boundary, the inherent image discretization of the boundary element method naturally describes the object being imaged. If a finite element technique were used, the entire domain would have to be discretized - increasing the computational load - despite the fact that the unknowns are only on the boundary. In addition, resolution and quality of the reconstructed images from a finite element method depends highly on the way the domain is discretized. A similar technique has been proposed by Duraiswami et al. [3] who considered a cubic region with spherical voids and measurements on all boundaries of the cube.

Image Reconstruction Procedure

As mentioned earlier, the region of interest can be thought of as a cylindrical conductor containing voids of zero conductivity. The electrodes are uniformly distributed on a circular band in the mid section of the cylinder (Fig. 1). This arrangement is particularly

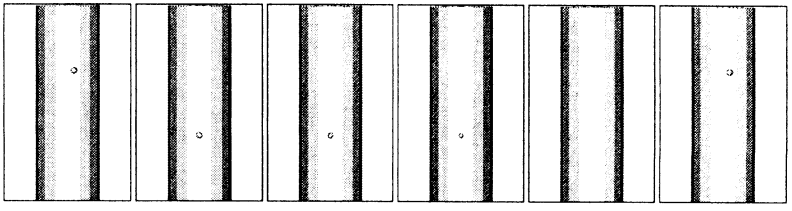


Figure 3: Images of the voids on the $x - z$ plane. Frame 1: original void, 2: initial guess, 3-5: intermediate, and 6: reconstructed void. The shape parameters are $x = 1, y = 1, z = 10$, $a_{00} = 0.5$ (original and reconstructed).

suitable for experimental verifications that may be pursued in the future.

The imaging procedure consists of applying a voltage pattern at the electrodes and reconstructing the void shapes from the measured currents at the electrodes. We idealize these steps by replacing electrodes with nodes on the boundary integral grid. In the forward problem, the basic task is to solve Laplace's equation for the potential ϕ representing the voltage in the cylindrical region,

$$\nabla^2 \phi = 0. \tag{1}$$

Here (z, r, ψ) are 3-D cylindrical coordinates with the origin located at the geometrical center of the cylinder. The domain of the problem is defined by $0 < r < R_c$ and $-L_c < z < L_c$ where R_c is the radius of the cylinder and $2L_c$ the length. The boundary conditions are given by $\phi = \cos\psi$ on C where C is defined by $r = R_c$ and $-L_e < z < L_e$ where $2L_e$ is the width of the electrode band. The normal derivative of ϕ, ϕ_n, is zero everywhere else on the cylinder surface. Since the voids do not conduct electricity, ϕ_n must be set to zero on their surfaces (T). The solution to (1) is obtained by a standard boundary integral formulation (for details see Oguz & Zeng [10]).

The voids are assumed to be discrete, spheroidal objects with moderate deformation so that a local spherical-coordinate system can adequately define their surfaces. The shape of each void is parameterized by the equation

$$\rho = \sum_{m=0}^{M_p} \sum_{n=m}^{N_t} \begin{pmatrix} a_{mn} \\ b_{mn} \end{pmatrix} P_n^m(\cos\theta) \begin{pmatrix} \cos m\Psi \\ \sin m\Psi \end{pmatrix} \tag{2}$$

where

$$\rho = \sqrt{(x - x_0)^2 + (y - y_0)^2 + (z - z_0)^2}.$$

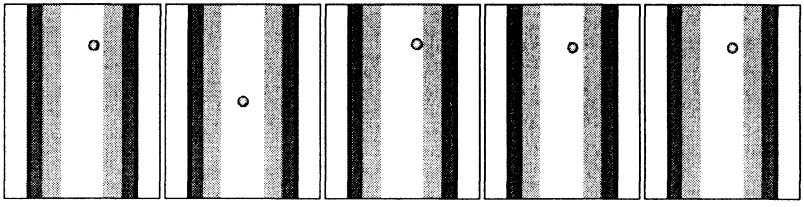


Figure 4: Images of the voids on the $x - z$ plane. Frame 1: original void, 2: initial guess, 3,4: intermediate, and 5: reconstructed void. The shape parameters are $x = 1, y = 1, z = 7$, $a_{00} = 0.5$ (original) and $x = 0.9446, y = 0.9122, z = 4.8443$, $a_{00} = 0.4928$ (reconstructed).

for $0 < \theta < \pi$, $0 < \Psi < 2\pi$. Here θ and Ψ are spherical coordinates with the origin at the geometrical center of the void (x_0, y_0, z_0), and ρ is the distance from the center of the void to a surface point (x, y, z). A similar shape parameterization using the Fourier on two-dimensional objects has been used by Han [5] and Han & Prosperetti [6]. The parameters $x_0, y_0, z_0, a_{mn}, b_{mn}$ define the shape of the object. In this study, we restrict a_{mn} and b_{mn} to just a_{00}, a_{02}, a_{22}, and b_{22} in addition to x_0, y_0, z_0. A conversion from the analytical description of the voids in (2) to a surface element representation is necessary for the target boundaries. This task is accomplished by radially mapping the nodes of a unit sphere to the void surface.

Our imaging algorithm is iterative and can be summarized by the following steps

(0) Start with an initial void shape.

(1) Compute ϕ_n at the electrodes (forward solution).

(2) Calculate the error, i.e. the difference between the computed and measured ϕ_n at the electrodes.

(3) Using the Levenberg-Marquardt algorithm, adjust the parameters of the void shape to minimize the error.

(4) Go to (1) if the change is greater than a certain minimum value

In the following section several numerical simulations of this algorithm are presented.

Simulations

In all the cases presented here, the cylinder is discretized by 304 linear-rectangular continuous-elements on its side wall (with 19 axial and 16 angular segments) and 64 linear-triangular continous-elements

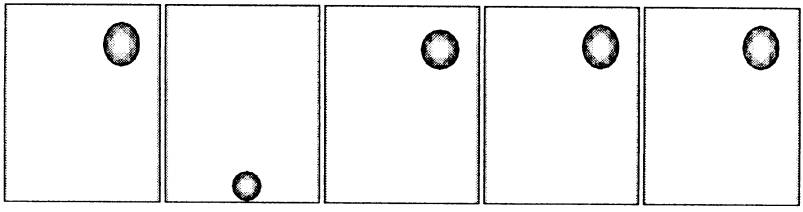


Figure 5: Images of the voids on the $x - z$ plane. Frame 1: original void, 2,3,4: intermediate, and 5: reconstructed void (initial guess at $x = y = z = 0$ is not visible). The shape parameters are $x = 1, y = 1, z = 5$, $a_{00} = 0.5$, $a02 = 0.05$ (original and reconstructed).

on its top and bottom surface. Voids are represented by 128 triangular elements with a total of 66 nodes. We also fixed the number of electrodes to 64 (16x4) boundary nodes and employed only one realization of the imposed electric pattern on the electrodes i.e. $\phi = \cos\psi$. The geometry of the cylinder is defined by $L_c = 40$, R_c=5 and $L_e = 5$ in dimensionless units.

In fig. 2 we show a typical case in which a single spherical void is present in the target space. The original void geometry is plotted in the first frame. The second and subsequent frames corresponds to the initial geometry and intermediate iterations of the void. The differences between the first and the last frame is virtually indistinguishable. Similar results are obtained for spherical voids of various radii and locations when the center of the void is inside the electrode band. Even when the void is far from the electrode band the algorithm detected it properly (fig. 3). In this case, the axial location of the void is $z = 10$ which is 5 unit lengths away from the nearest electrode. However, the detectability range decreases significantly if only four significant digits are kept in the measurements (fig. 4).

In fig. 5 a deformed sphere is successfully imaged from measurements with four significant digits. The match between the original void and the reconstructed one is very good. For the deformed voids, we have found that better results are obtained if we first assume that the void is spherical and let the algorithm compute its location and radius. After convergence we then iterate for the shape coefficients a_{02}, a_{22} and b_{22}. The computational time is slightly less with this scheme, and the inversion is more robust especially in the case of multiple voids. The trend has also been observed in the 2-D case of Han [5].

The simulations with two voids have yielded results equally as

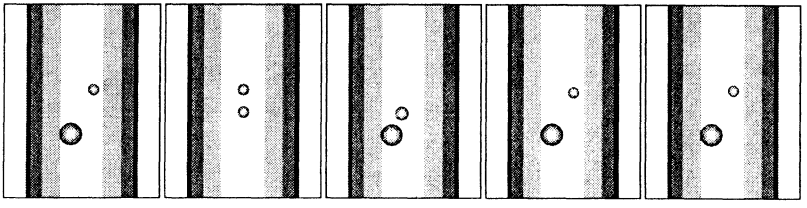


Figure 6: Images of the voids on the $x - z$ plane. Frame 1: original void, 2: initial guess, 3,4: intermediate, and 5: reconstructed void. The shape parameters are void 1: $x = 1, y = 1, z = 2$, $a_{00} = 0.5$ void 2: $x = -1, y = -1, z = -2$, $a_{00} = 1.0$ (original) and void 1: $x = 0.9835, y = 1.0047, z = 1.9897$, $a_{00} = 0.5008$ void 2: $x = -1.0030, y = -0.9992, z = -1.9983$, $a_{00} = 0.9998$ (reconstructed).

good as with single voids. In fig. 6 we show the original and reconstructed images of two spherical voids. A very close match between the original and reconstructed configuration of the voids is obtained in spite of the fact that four significant digits are kept in the measurements. The algorithm works equally well for deformed voids. A typical example is shown in fig. 7 where two deformed voids of different sizes are imaged successfully.

In this preliminary work, our efforts did not include voids of larger size. We have found that the voids need to be sufficiently apart for a successful inversion.

Conclusions

We have shown that a shape parameterization in conjunction with boundary integral technique is an effective imaging method for non-conductive objects in a three dimensional domain of uniform conductivity. The initial set of numerical simulations indicate that a single void can be imaged without any difficulty when its shape deviates moderately from a sphere. Remarkably, a void far from the measurement points can also be detected accurately as well even if the measurement accuracy is limited to four significant digits. The algorithm works equally well in the case of two voids. However, based on several trial cases, imaging three or more voids does not yield satisfactory results with the current technique. The results presented in this paper are obtained by using measurements from a single voltage pattern imposed on the electrodes. Although it only permits up to

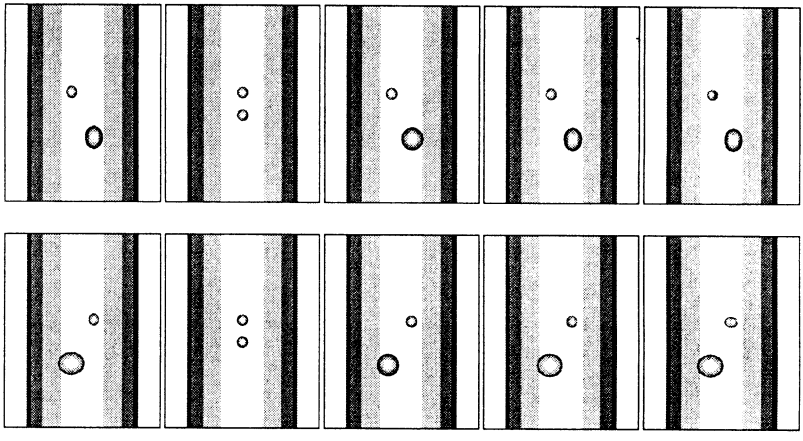


Figure 7: Images of the voids on the $y-z$ (1st row) and $x-z$ (2nd row) planes. Frame 1: original void, 2: initial guess, 3,4: intermediate, and 5: reconstructed void. The shape parameters are void 1: $x = 1, y = 1, z = 2$, $a_{00} = 0.5$, $a_{02} = 0.05$ void 2: $x = -1, y = -1, z = -2$, $a_{00} = 1.0$, $a_{22} = 0.05$ (original) and void 1: $x = 0.8482, y = 0.8704, z = 1.9700$, $a_{00} = 0.4900$, $a_{02} = -0.0216$, $a_{22} = 0.0275$, $b_{22} = 0.0398$, void 2: $x = -1.0049, y = -1.0093, z = -2.0049$, $a_{00} = 0.9987$, $a_{02} = 0.0209$, $a_{22} = 0.0603$, $b_{22} = -0.0019$ (reconstructed).

two voids in the domain, using a single voltage pattern enables the current technique to be a fast image reconstruction.

Acknowledgment

Support for this work by the Office of Naval Research is gratefully acknowledged.

References

[1] M. Cheney and D. Isaacson. Noser: An algorithm for solving the inverse conductivity problem. *Int. J. Imaging Systems Tech.*, 2:66–75, 1990.

[2] K.A. Dines and R.J. Lytle. Analysis of electrical conductivity imaging. *Geophysics*, 46:1025–1036, 1990.

[3] R. Duraiswami, G.L. Chahine, and K. Sarkar. Boundary element techniques for efficient 2-d and 3-d electrical impedance tomography. *Chem. Eng. Sci.*, 52:2185, 1997.

[4] R. Guardo, C. Boulay, B. Murray, and M. Bertrand. An experimental study in electrical impedance tomography using back-projection reconstruction. *IEEE Trans. Biomed. Eng.*, BME-38:617–627, 1991.

[5] D. Han. *Shape decomposition technique in electrical impedance tomography (EIT).* PhD thesis, Johns Hopkins University, Dept. of Mechanical Engineering, 1997.

[6] D. Han and A. Prosperetti. Shape decomposition technique in electrical impedance tomography. *in preparation*, 1998.

[7] O.C. Jones, J.T. Lin, H. Shu, L. Ovacik, and Y. He. Impedance imaging relative to binary mixtures. *ASME FED Liquid-Solid Flows*, 189:91–101, 1994.

[8] M. Murai and Y. Kagawa. Boundary element iterative technique for determining the interface boundary between two laplace domains - a basic study of impedance plethymography as an inverse problem. *Int. J. Numer. Methods Eng.*, 23:35–47, 1985.

[9] M. Murai and Y. Kagawa. Electrical impedance computed tomography based on a finite element model. *IEEE Trans. Biomed Eng.*, BME-32:177–184, 1985.

[10] H.N. Oguz and J. Zeng. Axisymmetric and three-dimensional boundary integral simulations of bubble growth from an underwater orifice. *Eng. Analysis with Boundary Elements*, 19:319–330, 1997.

[11] B.F. Wexler and M.R. Newman. Impedance-computed tomography algorithm and system. *applied Optics*, 24:3985–3992, 1984.